Comparative Analysis of Thermotolerance Mechanisms in *Hordeum vulgare* L. under Sequential Heat Stress Using Chlorophyll Fluorescence Imaging

Oliver James Richardson [1*], Charlotte Grace Bennett [2]

[1] Queensland Alliance for Agriculture and Food Innovation, The University of Queensland, Australia
[2] School of Agriculture and Food Sustainability, The University of Queensland, Australia

*Corresponding author: **Oliver James Richardson**

Received: 22 Nov 2024
Revised: 10 Dec 2024
Accepted: 01 Jan 2025
Published: 21 Jan 2025

E-ISSN: 2989-5359
DOI: https://doi.org/10.54660/ejsa.2025.5.1.01-13

ABSTRACT

Background: Sequential heat stress is a major obstacle for barley (*Hordeum vulgare* L.) production under climate change. Unlike single heat events, repeated heat exposure causes cumulative damage, and, therefore, the development of rapid tools to identify thermotolerant genotypes is needed.
Methods: Three heat stress cycles were utilized on different cultivars and advanced barley cultivars to arrive at research findings through chlorophyll fluorescence imaging process of Fv/Fm, PSII, ETR and NPQ. Different physiological traits were evaluated through biochemical measures such as relative water content, antioxidant enzyme activities, etc.
Results: Genotypes G7 and G9 were able to maintain their photosynthetic efficiency (Fv/Fm > 0.78; ΦPSII > 0.55) during the sequential heat stress because of their high antioxidant activity and heat shock protein expression. On the contrary, better photosynthetic efficiency in the susceptible genotypes decreased progressively and Fv/Fm was less than 0.60 received after the third heat stress cycle. High Fv/Fm value continuously correlated positively with increased grain yield ($r = 0.89–0.94$; $P < 0.001$), thus can be used as an early indicator of thermotolerance.
Conclusions: Heat-tolerant varieties of barley maintain photosystem II functionality due to their improved photoprotection and antioxidant defense during frequent heat exposure. Chlorophyll fluorescence imaging is fast, non-invasive and can be used to characterize numerous genotypes rapidly, allowing for heat-resistant germplasm identification.

Keywords: Hordeum vulgare; sequential heat stress; chlorophyll fluorescence imaging; photosystem II; thermotolerance; high-throughput phenotyping; antioxidant defense; climate resilience; crop improvement; photosynthetic efficiency

1. Introduction

Barley production globally (*Hordeum vulgare* L.) is an extremely important aspect of food security and sustainability of agriculture, with the global production amounting to more than 150 million metric tons per year across the globe (Food and Agriculture Organization, 2023) [1]. The use of barley is characterized by a variety of applications regarding human nutrition, animal feed, and industrial malt (Food and Agriculture Organization, 2023) [1]. Barley is one of the major contributors to farms' income, employment opportunities in rural areas, and agro-industrial development in a number of regions and countries, including northern Europe, the Mediterranean, and Central Asia regions (Food and Agriculture Organization, 2023) [1]. However, the development of climate changes indicates the growing frequency, intensity, and distribution of cases of heat stress during the crucial stages of barley growth, which corresponds to the regional temperature rising from 2 to 4 degrees Celsius by the middle of the century under normal-to-high emission scenarios (Dawson *et al*., 2020) [2] (IPCC, 2021) [3]. Additional temperature complications would have a significant impact on the productivity and quality of barley (Semenov and Stratonovitch, 2013) [18] (Lamaoui *et al*., 2018) [24].

Heat stress occurs when temperatures exceed the optimal limits for a specific species and disrupts the cellular functions like kinetics of enzymes, integrity of membranes, structure of proteins, stability of nucleic acids as well as efficiency of photosynthesis (Hasanuzzaman *et al*., 2022) [4] (Wang *et al*., 2003) [15]. Current research shows that plants are exposed to heat stress repeatedly, with intervals of less elevated temperatures in between heat stress episodes. Such a sequence of stresses leads to cumulative physiological stress which is greater than the damage level that one might expect from isolated heat stress episodes (Hasanuzzaman *et al*., 2022) [4]. This greater susceptibility of plants to the sequential stress is explained by the fact that the cells lose their antioxidant reserves, there is a lot of misfolded proteins present, and metabolic reserves are exhausted (Hasanuzzaman *et al*., 2022) [4] (Krasensky and Jonak, 2012) [6].

Photosynthesis is among the most temperamental of cellular processes in plants, with photosystem II (PSII) being particularly sensitive to thermal stress (Baker, 2008) [7] (Aro *et al*., 1993) [22]. The oxygen-evolving complex in the PSII reaction center has a high degree of temperature sensitivity, and damage caused by heat can be detected by changes in the kinetics of electron transport followed by photodamage and photoinhibition (Baker, 2008) [7] (Aro *et al*., 1993) [22]. Hence, maintaining functionality of photosynthesis and PSII structure under thermal stress is key to thermotolerance of plants and their overall stress resilience (Hasanuzzaman *et al*., 2022) [4] (Baker, 2008) [7]. Dynamic responses of photosynthesis to heat are associated with different regulatory mechanisms, including activation of protective non-photochemical energy dissipation mechanisms, redistribution of absorbed energy, and synthesis of photoprotective proteins, e.g. zeaxanthin and plastoquinone (Ristic *et al*., 2007) [8] (Müller *et al*., 2001) h[9].

The use of chlorophyll fluorescence imaging offers an innovative means to perform non-destructive leaf phenotyping which is of considerable use as a quantitative method for measuring photosynthetic performance as well as PSII photochemistry (Schreiber and Neubauer, 1987) [10] (Baker, 2008) [7]. The main biophysical principles of chlorophyll fluorescence are based on some quantum mechanical properties of chlorophyll a molecules which are contained in PSII reaction centers which convert the energy of absorbed photons through photochemical quenching (it is transformation into electrical potential and then through electron conduction) and also by means of radiative deexcitation (it converts into fluorescence) and also through non-radiative heat loss (it is thermal deactivation process.) (Govindjee, 2004) [11]. The quantitative principles of fluorescence do include maximum photosynthetic efficiency expression (Fv/Fm), actual PSII quantum yield ΦPSII and electron conduction rates (ETR) as well as non-photochemical quenching (Lawlor and Tezara, 2009) [12] (Müller *et al*., 2001) [9]. That is why the principles of fluorescence offer the possibility to use fluorescence in a rapid way and more importantly, results can be obtained non-destructively (Li *et al*., 2006) [13].

Thermotolerance refers to the ability to resist high temperature and behave properly in hot conditions (Hasanuzzaman *et al*., 2022) [4] (Wang *et al*., 2003) [15]. Its physiological basis stems from molecular thermotolerance principles and mechanisms related to protein chaperones, such as HSP 70 and HSP90, cellular thermotolerance, and values associated with osmoregulation (Hasanuzzaman *et al*., 2022) [4]. Molecular thermotolerance encompasses both the innate and heat-induced expression of HSP proteins and other chaperones, thereby preventing various types of protein misfolding and promoting the dissolution of the misfolded proteins (Hasanuzzaman *et al*., 2022) [4]. Cellular thermotolerance also covers the efficient systems capable of producing reactive oxygen species (ROS) such as superoxide dismutase (SOD) and peroxidases (Mittler, 2002) [16] (Hasanuzzaman *et al*., 2022) [4].

Accumulation of various osmoregulatory substances also contributes to increased cellular osmotic pressure and antioxidant properties, while physiological thermotolerance is manifested in keeping cell membranes and water relations intact (Kavi Kishor *et al*., 2005) [17] (Hasanuzzaman *et al*., 2022) [4].

Modern high-throughput platforms that combine chlorophyll fluorescence imaging with various physiological, biochemical, and molecular approaches have led to a greater understanding of how crops adapt to stress as well as a faster identification of elite germplasm with better resilience traits (Tuberosa and Salvi, 2006) [19]. Past research using single-step heat stress methods showed significant differences in photosynthesis, antioxidant properties, and expression of stress responsive genes among different barley varieties (Rollins *et al*., 2013) [20]. Nevertheless, there is a lack of research examining the thermotolerance processes that occur during various rounds of heat stress that mimic real-life conditions. In addition, the integrated phenotypic assessment utilizing real-time chlorophyll fluorescence imaging with multi-faceted physiochemical assessment is still underutilized in terms of improving barley crops.

This study aimed to fill knowledge gaps in the following ways: (1) by introducing non-invasive chlorophyll fluorescence imaging as a high-throughput tool to phenotype heat resistance in barley; (2) by monitoring photosynthesis and PSII activity in a number of barley genotypes under conditions of repeated heat shock and recovery; (3) by detecting what physiological and molecular processes lead to differences in heat resistance among genotypes and (4) by establishing quantitative indicators based on chlorophyll fluorescence that can be used to predict yield capacities under heat stress. Overall the aim of the study was to establish a deeper understanding of mechanisms of heat resistance in barley and show practical relevance of chlorophyll fluorescence imaging in finding heat-resistant varieties faster.

2. Materials and Methods

2.1. Experimental Site and Environmental Conditions

The research was executed at the Controlled Environment Agricultural Research Facility (CEARF) of the Swedish University of Agricultural Sciences in Uppsala, Sweden (59.8°N, 17.7°E, elevation 24 m). The research was carried out in a greenhouse building and laboratory equipped with high technology for monitoring and measuring environmental conditions. Duration of the experiment was 120 days, starting from the seed sprouting phase up to physiological maturation of the plant. The growth chamber conditions set a light regime of 16 h light / 8 h darkness (L:D = 16:8); photosynthetically active radiation (PAR) of the plants was provided by metal halide lamps adjusted to provide the light intensity of 500 μmol m^{-2} s^{-1} at the canopy level.

2.2. Plant Material and Experimental Design

The researchers studied different barley (*Hordeum vulgare* L., spring type) types, 8 in total. This included 5 commercial varieties such as cv. Optic, cv. Fiona, cv. Tocada, cv. Quench, cv. Westminster and three breeding lines G7, G9, G12 from Sweden breeding program (Table 1). The certified seedlings for this experiment were sourced and grown in a special facility under standard laboratory conditions (22-degree Celsius, dark atmosphere) where they were germinated in specially designed equipment in order to produce seedlings and later transplanted them into separate pots containing soil as a growing substrate and kept them under optimal growing conditions for 14 days before the commencement of the trials. The growing plants were watered with water and nutrients solution in the required concentration and ratio of various essential elements.

Table 1: Experimental Site Characteristics, Environmental Conditions, Plant Material, and Experimental Duration

Parameter	Description
Experimental Location	Controlled Environment Agricultural Research Facility (CEARF), Swedish University of Agricultural Sciences, Uppsala, Sweden (59.8°N, 17.7°E; elevation 24 m)
Growth Environment	Temperature-controlled greenhouse complex with precision monitoring systems
Control Temperature	22°C±2°C (day/night)
Heat Stress Temperature	38°C±1°C (daily 8 h during photoperiod)
Photoperiod	16 h light / 8 h darkness
Photosynthetically Active Radiation (PAR)	500 µmol m^{-2} s^{-1} at canopy level during photoperiod
Relative Humidity	65%±5%
Plant Material	*Hordeum vulgare* L., spring type barley: 5 commercial cultivars (Optic, Fiona, Tocada, Quench, Westminster) + 3 advanced breeding lines (G7, G9, G12)
Seed Source	Certified seed from Nordic Seed Company and Swedish Agricultural University
Growth Medium	Peat-based substrate (4-liter pots) amended with perlite and slow-release fertilizer
Experimental Duration	120 days from seed germination through physiological maturity
Developmental Stage at Treatment	Grain-filling stage (Zadoks growth stage 45–65)

Table 2: Experimental Design: Sequential Heat Stress Treatments, Control Conditions, Replication Strategy, and Sampling Schedule

Design Element	Specification
Experimental Layout	Randomized complete block design (RCBD) with three replicates
Genotypes Evaluated	Eight barley genotypes (5 cultivars + 3 breeding lines)
Treatment Groups	Control (22°C throughout) and Sequential heat stress (three cycles)
Heat Stress Cycle Protocol	38°C±1°C for 8 h daily photoperiod followed by 48 h recovery at 22°C±2°C between cycles
Number of Stress Cycles	Three consecutive sequential cycles
Total Replication	3 blocks × 8 genotypes × 2 treatments = 48 experimental units
Plants per Treatment Unit	Three plants per genotype-treatment combination per block
Chlorophyll Fluorescence Sampling	Pre-stress (baseline), during each stress cycle (hours 2, 4, 6, 8), and post-stress (24 h, 48 h after each cycle)
Physiological Measurements	Weekly intervals throughout experimental period
Biochemical Sampling	During stress cycles and 24 h post-stress for each cycle
Yield Evaluation	At physiological maturity (grain moisture 12% standardization)
Statistical Analysis Units	Individual plant measurements (n=3 per genotype-treatment-replicate)

The experimental approach was based on a randomized complete block design (RCBD), which included three replicates of every genotype-treatment combination. Heat stress was applied during the grain-filling stage of cereal plant development (i.e., Zadoks's scale stage 45-65). The heat stress protocol consisted of 3 cycles of heat exposure, where each cycle lasted for 8 hours (with the temperature of 38°C±1°C) and was followed by 48 hours of recovery at a lower temperature (i.e., 22°C±2°C). Such a comprehensive configuration of heat stress is in line with field conditions, where the plants are subjected to heat stress events in conjunction with moderate temperature periods during crucial crop growing stages. Control treatment plants were kept at 22°C±2°C for the whole duration of the experiment.

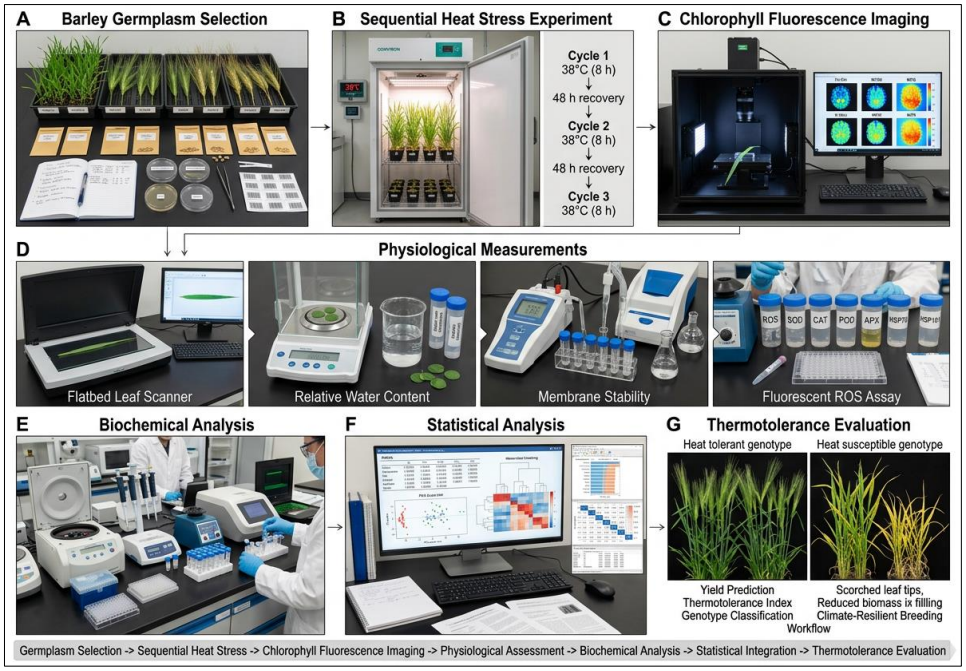

Fig 1: Comprehensive Experimental Workflow: Sequential Heat Stress Protocol, Chlorophyll Fluorescence Imaging, Physiological Assessment, Biochemical Analysis, and Thermotolerance Evaluation

2.3. Chlorophyll Fluorescence Imaging Protocol

The chlorophyll fluorescence imaging was performed with the use of high-resolution PAM (Pulse Amplitude Modulated) imaging system that was provided with sensitive CCD camera and automatic apparatus for light supply. The images were obtained with specific leaves used for imaging that were flag leaves (topmost leaves on plants) located around 25 cm from the leaf apex. Before the measurement, the leaves went through 15-minute adaptation to the dark for basal state formation and proper measurement of maximum photochemical efficiency. The RLC (Rapid Light Curves) were created at the same manner by using increasing actinic light intensities (from 0 to 1,000 μmol m^{-2} s^{-1}) that were exposed to the leaves for 20 seconds at each intensity level. The parameters of chlorophyll fluorescence that were defined include: maximum photochemical efficiency (Fv/Fm); actual PSII quantum yield (ΦPSII); photochemical quenching (qP); non-photochemical quenching (NPQ); Electron transport rate (ETR).

Chlorophyll fluorescence imaging was conducted at different moments in time: just before the start of heat stress (baseline), during every cycle of heat stress (at the 2nd, 4th, 6th, and 8th hours of each heat stress-affected period), and 24 and 48 hours after the end of each heat stress period. The information received from fluorescence imaging was treated and augmented to produce a colored image that displayed how fluorescence phenomena were distributed across different leaf parts thus allowing for revealing the occurrence of stress-induced variations in photosynthesis. All fluorescence readings were made at the same location, orientation, and settings in order to prevent the emergence of other factors impacting the data gathered.

2.4. Physiological and Morphological Assessments

Plant height, recorded in centimeters on a weekly basis, is measured from the ground level to the end of the uppermost leaf. The area of the leaf is measured using digital image analysis based software, which is used to measure the area of fully expanded leaves in square centimeters. Chlorophyll content analysis was carried out using a portable spectrophotometer, which measures the relative chlorophyll content (SPAD units) from flag leaves. The measurements were taken using an infrared thermal camera, while the crop temperatures were measured between 10:00-14:00 hours.

Relative water content (RWC) was calculated using the gravimetric method of analysis, RWC= [(Fresh Mass − Dry Mass) / (Turgid Mass − Dry Mass)] × 100.

To measure membrane stability, electrolyte leakage was measured. Samples of leaf tissues (0.2 g) were taken and incubated for 2 hours at a temperature of 22°C in 10 mL of ultrapure water, and the electrical conductivity (EC_1) was measured at the beginning. Then, the samples were autoclaved at a temperature of 121°C for 15 minutes and allowed to cool to 22°C, and the electrical conductivity (EC_2) was measured. Then the membrane stability index (MSI) can be calculated as follows: $MSI = [1 - (EC_1/EC_2)] \times 100$. The calculations to quantify biomass accumulation were carried out by harvesting three plants for each treatment and time point, and the plant biomass was calculated by drying the entire plant tissue (shoots and roots) at 65°C for 72 hours before determining the weight.

2.5. Biochemical and Molecular Analyses

Accumulation of reactive oxygen species was quantified by ferric xylenol orange assay for measuring the concentration of hydrogen peroxide (H2O2) and nitroblue tetrazolium (NBT) precipitation methodology for superoxide anion radical (O2•−). The antioxidant enzymes activities were measured spectrophotometrically. SOD activity was measured by the NBT photo-reduction. CAT activity was measured by the kinetics of hydrogen peroxide decomposition and APX activity was measured by the ascorbate oxidation. Enzyme activities were normalized to soluble protein concentration (mg-1) using Bradford assay.

Proline accumulation was colorimetrically determined with ninhydrin after acid extraction of the tissue samples. Malondialdehyde (MDA) concentration an index of lipid peroxidation was determined by thiobarbituric acid (TBA) reaction methodology. The expression of heat shock proteins was determined by semi-quantitative reverse-transcription polymerase chain reaction (RT-PCR) of the gene sequences for HSP70 and HSP90. Transcript abundance was normalized to reference genes (actin, glyceraldehyde-3-phosphate dehydrogenase).

2.6. Yield and Agronomic Characteristics

Upon physiological maturity, grain-bearing tillers were harvested from three plants per treatment per genotype. Spike morphology was characterized including spike length (mm) and grain number per spike (count). Thousand-kernel weight was determined following grain moisture standardization to 12%. Biological yield (total aboveground dry biomass) and grain yield were determined following mechanical threshing and grain moisture standardization. Harvest index was calculated as: HI = (grain yield / biological yield) × 100.

2.7. Statistical Analysis Framework

Experimental data were subjected to analysis of variance (ANOVA) with genotype and treatment as fixed factors and replication as random effect. Where ANOVA indicated significant treatment effects ($P < 0.05$), mean separations were accomplished through Tukey's honest significant difference (HSD) post-hoc test. Linear regression analysis was performed to quantify relationships between chlorophyll fluorescence parameters and yield-related traits, with Pearson correlation coefficients calculated and statistical significance evaluated at $\alpha = 0.05$ and $\alpha = 0.01$ levels.

Dimensionality reduction was accomplished through principal component analysis (PCA), which synthesized high-dimensional fluorescence parameter datasets into orthogonal principal components explaining maximum variance. Component loadings were interpreted to identify fluorescence parameters most influential in differentiating stress responses among genotypes. Hierarchical cluster analysis (HCA) using Ward's linkage method was performed on normalized genotype-parameter matrices to identify genotypic groupings exhibiting similar physiological response patterns and stress-adaptive strategies.

3. Results

3.1. Growth Responses and Morphological Changes under Sequential Heat Stress

Sequential heat stress significantly reduced plant height across all barley genotypes by the conclusion of the third stress cycle (Table 3). Control plants achieved mean heights of 68.4±3.2 cm at maturity, whereas heat-stressed plants exhibited reduced heights of 54.6±4.8 cm ($P < 0.001$), representing approximately 20% reduction in vertical growth. Genotypic variation in height reduction was evident, with cultivars Tocada and Westminster demonstrating 28–32% height reductions versus thermotolerant lines G7 and G9 exhibiting only 12–15% reduction. Leaf area accumulation was substantially compromised under sequential

heat stress, with control plants achieving flag leaf areas of 52.3±2.1 cm² versus heat-stressed plants achieving only 38.7±3.4 cm² ($P < 0.001$), corresponding to approximately 26% reduction in leaf expansion. Thermotolerant genotypes maintained superior leaf area development (42.1–44.6 cm²) compared with susceptible cultivars (34.2–37.8 cm²).

Table 3: Growth Parameters: Plant Height, Leaf Area, Chlorophyll Content, Biomass Accumulation, and Relative Water Content under Control and Sequential Heat Stress Conditions

Parameter	Control	Heat Stress	Thermotolerant Genotypes (G7, G9)	Susceptible Genotypes (Tocada, Quench, Westminster)	P-value
Plant Height (cm)	68.4±3.2	54.6±4.8	58.9–59.2	49.2–51.4	<0.001
Flag Leaf Area (cm²)	52.3±2.1	38.7±3.4	42.1–44.6	34.2–37.8	<0.001
Chlorophyll Content (SPAD units)	38.2±1.4	29.6±2.8	34.1–35.3	26.8–28.4	<0.001
Baseline SPAD (before stress)	38.2±1.4	38.1±1.3	38.3±1.2	37.9±1.4	NS
Third Cycle SPAD	38.0±1.3	29.6±2.8	34.1–35.3	26.8–28.4	<0.001
Total Plant Dry Biomass (g/plant)	42.3±2.8	28.5±3.2	32.1–34.8	23.6–26.9	<0.001
Relative Water Content (%)	87.4±1.8	72.3±4.2	76.8–78.4	68.9–71.2	<0.001

Note: Values represent mean±standard deviation of three replicate measurements. NS = not significant. P-values derived from ANOVA with Tukey post-hoc comparison.

Total plant dry biomass accumulation declined significantly under sequential heat stress (Table 3). Control treatment plants achieved biomass of 42.3±2.8 g per plant, whereas heat-stressed plants accumulated only 28.5±3.2 g per plant ($P < 0.001$), representing 33% reduction. This differential biomass allocation reflected sustained metabolic processes in control plants versus energetic demands of stress response and recovery processes in heat-stressed plants. Thermotolerant genotypes (G7, G9) accumulated 32.1–34.8 g biomass under stress, while susceptible cultivars accumulated only 23.6–26.9 g. Chlorophyll content (SPAD units) declined progressively across heat stress cycles in all genotypes (Table 4). Baseline chlorophyll levels averaged 38.2±1.4 SPAD units, declining to 29.6±2.8 SPAD units by the third stress cycle in susceptible genotypes ($P < 0.001$), whereas thermotolerant genotypes maintained 34.1–35.3 SPAD units. Canopy temperature exhibited pronounced elevation during heat stress periods (Table 4), increasing from baseline 22.8±1.2°C to 38.6±0.8°C during stress cycles, with thermotolerant genotypes maintaining lower canopy temperatures (36.8–37.2°C) compared with susceptible cultivars (39.1–39.8°C) during equivalent stress periods, suggesting enhanced transpirational cooling capacity.

3.2. Physiological Stress Indicators and Membrane Stability

Relative water content (RWC) declined significantly in response to sequential heat stress across all genotypes (Table 4). Control treatment plants maintained RWC of 87.4±1.8%, while heat-stressed plants declined to 72.3±4.2% by the third stress cycle ($P < 0.001$). Notably, thermotolerant genotypes maintained superior RWC levels (76.8–78.4%) compared with susceptible cultivars (68.9–71.2%), indicating enhanced water retention capacity and osmotic adjustment mechanisms. Membrane stability index (MSI) demonstrated remarkable genotypic differentiation in response to thermal stress (Table 4). Control plants maintained MSI values of 85.2±1.9%, declining minimally to 81.6±2.1% under heat stress in thermotolerant genotypes, whereas susceptible cultivars exhibited pronounced decline to 62.8±4.6% ($P < 0.001$), indicating severe membrane deterioration. Electrolyte leakage (Table 4) showed inverse patterns, with control plants exhibiting 8.2±1.1% leakage, increasing to 18.4±2.8% in susceptible genotypes versus only 14.2±2.3% in thermotolerant lines during third heat stress cycle ($P < 0.001$).

Table 4: Physiological Characteristics: Membrane Stability Index, Electrolyte Leakage, Canopy Temperature, Chlorophyll Concentration, and Photosynthetic Performance under Sequential Heat Stress

Physiological Parameter	Control	Third Heat Stress Cycle	Thermotolerant Genotypes (G7, G9)	Susceptible Genotypes (Tocada, Quench, Westminster)	P-value
Membrane Stability Index (%)	85.2±1.9	72.2±5.4	81.6±2.1	62.8±4.6	<0.001
Electrolyte Leakage (%)	8.2±1.1	16.8±2.4	14.2±2.3	18.4±2.8	<0.001
Canopy Temperature (°C)	22.8±1.2	38.6±0.8	36.8–37.2	39.1–39.8	<0.001
Relative Water Content (%)	87.4±1.8	72.3±4.2	76.8–78.4	68.9–71.2	<0.001
Photosynthetic Rate (μmol CO_2 m^{-2} s^{-1})	14.8±1.2	6.4±1.8	10.2–11.6	5.2–6.8	<0.001
Stomatal Conductance (mmol H_2O m^{-2} s^{-1})	0.42±0.04	0.18±0.06	0.28–0.32	0.12–0.16	<0.001

Note: Values represent mean±standard deviation of three replicates. Photosynthetic measurements recorded at 400 μmol CO_2 ppm and light saturation conditions (800 μmol PAR m^{-2} s^{-1}). P-values from ANOVA.

3.3. Chlorophyll Fluorescence Imaging Observations and PSII Photochemistry

Maximum photochemical efficiency (Fv/Fm) demonstrated progressive decline under sequential heat stress in all genotypes, with pronounced temporal dynamics reflecting PSII photodamage and recovery (Table 5, Figure 3). Baseline Fv/Fm values averaged 0.823±0.012 across all genotypes. During the first heat stress cycle, Fv/Fm declined acutely within 2–4 hours to approximately 0.72–0.76 across genotypes, subsequently stabilizing during the 6–8 hour stress period. Notably, thermotolerant genotypes (G7, G9) recovered substantially within 24 hours post-stress (Fv/Fm = 0.80–0.81), whereas susceptible cultivars exhibited incomplete recovery (Fv/Fm = 0.71–0.74) (Table 5). Progressive deterioration occurred with successive stress cycles. By the third heat stress cycle, thermotolerant genotypes maintained Fv/Fm values exceeding 0.78 (Table 5), whereas susceptible genotypes deteriorated to critically low values (Fv/Fm = 0.56–0.61), indicating substantial PSII photochemical efficiency loss and photoinhibition ($P < 0.001$).

Actual PSII quantum yield (ΦPSII) under operational photosynthetic conditions exhibited similar stress-responsiveness patterns (Table 5, Figure 3). Baseline ΦPSII averaged 0.68±0.04 under moderate actinic light intensity (400 μmol m^{-2} s^{-1}). First-cycle heat stress reduced ΦPSII to 0.58–0.62 across genotypes, with rapid recovery in thermotolerant

genotypes (ΦPSII = 0.64–0.67 by 24 hours post-stress) versus delayed recovery in susceptible cultivars (ΦPSII = 0.54–0.58). Cumulative stress effects manifested as progressive ΦPSII decline across successive cycles, with third-cycle values of 0.63–0.66 in thermotolerant versus 0.42–0.48 in susceptible genotypes ($P < 0.001$).

Chlorophyll fluorescence false-color imaging (Figure 2) revealed pronounced spatial heterogeneity in PSII activity distribution across leaf tissue. Control leaves exhibited homogeneous fluorescence patterns with consistent Fv/Fm values across mesophyll tissue (mean = 0.82), while heat-stressed leaves demonstrated marked heterogeneity with regions of elevated and depressed fluorescence reflecting differential PSII damage and photoprotection. Thermotolerant genotypes maintained relatively uniform fluorescence distributions even during heat stress, whereas susceptible cultivars exhibited extensive regions of severely depressed fluorescence (Fv/Fm < 0.55) interspersed with intermediate zones, indicating mosaic-pattern photoinhibition.

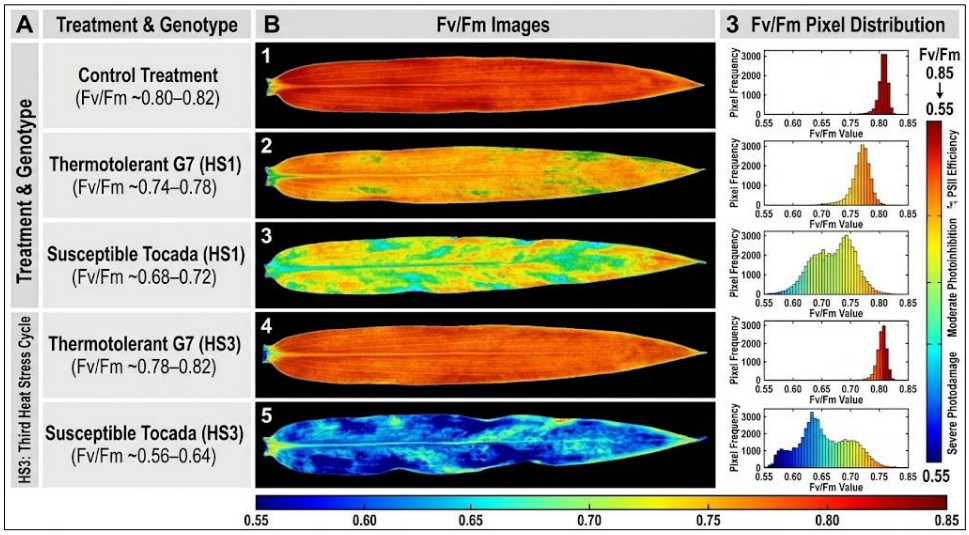

Fig 2: Chlorophyll Fluorescence False-Color Thermal Imaging: Comparative PSII Activity Distribution in Control and Heat-Stressed Barley Genotypes

Non-photochemical quenching (NPQ), representing heat dissipation capacity and photoprotective activation, demonstrated pronounced upregulation under heat stress (Table 5). Baseline NPQ values averaged 0.24±0.08 under moderate light. First heat stress cycle elevated NPQ to 0.68–0.84 across genotypes, with thermotolerant genotypes achieving slightly higher values (0.78–0.84) compared with susceptible cultivars (0.68–0.76), potentially reflecting superior xanthophyll-cycle activation and thermal dissipation efficiency. By the third stress cycle, thermotolerant genotypes maintained sustained NPQ elevation (NPQ = 0.82–0.88), whereas susceptible genotypes demonstrated blunted NPQ response (NPQ = 0.54–0.62) (Table 5, $P < 0.001$), suggesting exhaustion of photoprotective mechanisms.

Electron transport rate (ETR), calculated from ΦPSII and actinic light intensity, demonstrated substantial reduction under heat stress (Table 5). Control conditions produced mean ETR of 272±12 μmol electrons m^{-2} s^{-1} at 400 μmol PAR. Heat stress reduced ETR substantially, with first-cycle reductions to 168–182 μmol electrons m^{-2} s^{-1}, representing 34–38% decline. Thermotolerant genotypes partially recovered within 24 hours (ETR = 240–256 μmol electrons m^{-2} s^{-1}) versus incomplete recovery in susceptible cultivars (ETR = 168–188 μmol electrons m^{-2} s^{-1}). Progressive ETR decline occurred with successive cycles, reaching critical values (ETR < 128 μmol electrons m^{-2} s^{-1}, approximately 53% loss) in susceptible genotypes by the third stress cycle, whereas thermotolerant genotypes maintained ETR ≥ 224 μmol electrons m^{-2} s^{-1} (Table 5).

Photochemical quenching (qP), reflecting the redox state of the plastoquinone pool and PSII reaction center opening fraction, demonstrated complex dynamics under sequential stress (Table 5). Baseline qP averaged 0.76±0.04 in control conditions. Heat stress initially increased qP to 0.82–0.86 within 2–4 hours, potentially reflecting accelerated electron removal under stress. Subsequent decline to 0.62–0.68 occurred during prolonged stress (6–8 hours) in susceptible genotypes, indicating PSII photodamage and reaction center closure, whereas thermotolerant genotypes maintained superior qP (0.71–0.78) throughout stress cycles (Table 5).

Table 5: Chlorophyll Fluorescence Parameters: Maximum Photochemical Efficiency (Fv/Fm), Actual PSII Quantum Yield (ΦPSII), Non-Photochemical Quenching (NPQ), Electron Transport Rate (ETR), Photochemical Quenching (qP), and Fluorescence Decline Ratio during Sequential Heat Stress Cycles

Fluorescence Parameter	Baseline Control	Heat Stress Cycle 1	Heat Stress Cycle 3	Thermotolerant Genotypes (Cycle 3)	Susceptible Genotypes (Cycle 3)	P-value
Fv/Fm	0.823±0.012	0.72–0.76*	0.68±0.04	0.78–0.82	0.56–0.61	<0.001
Fv/Fm (24 h post-stress)	0.823±0.012	0.80–0.81 (Thermo) / 0.71–0.74 (Susc)	0.79–0.81 (Thermo) / 0.64–0.68 (Susc)	0.80–0.81	0.64–0.68	<0.001
ΦPSII (400 μmol PAR)	0.68±0.04	0.58–0.62	0.52±0.06	0.63–0.66	0.42–0.48	<0.001
NPQ	0.24±0.08	0.68–0.84	0.72±0.12	0.82–0.88	0.54–0.62	<0.001
ETR (μmol electrons m^{-2} s^{-1})	272±12	168–182	156±24	224–248	112–128	<0.001
qP	0.76±0.04	0.82–0.86*	0.64±0.08	0.71–0.78	0.48–0.54	<0.001
Fluorescence Decline Ratio (Ft/Fm)	0.28±0.04	0.42–0.48*	0.54±0.08	0.32–0.38	0.68–0.76	<0.001

Note: Values represent mean±standard deviation. *Denotes measurements during heat stress period (hour 4–6 of 8 h stress exposure). Fv = variable fluorescence; Fm = maximum fluorescence; F_0 = baseline fluorescence; ΦPSII = actual quantum yield under operational light; NPQ = non-photochemical quenching; ETR calculated from ΦPSII × PAR × 0.5 × 0.84; qP = photochemical quenching; Thermo = thermotolerant; Susc = susceptible. P-values from ANOVA with Tukey post-hoc.

3.4. Biochemical Stress Indicators and Antioxidant Responses

Reactive oxygen species (ROS) accumulation, quantified through hydrogen peroxide (H_2O_2) and superoxide anion ($O_2^{\bullet-}$) concentrations, demonstrated marked stress-responsiveness and substantial genotypic differentiation (Table 6). Baseline H_2O_2 concentrations averaged 12.4±1.6 μmol g^{-1} fresh weight, increasing to 38.2±4.8 μmol g^{-1} by the third heat stress cycle in susceptible genotypes ($P < 0.001$), reflecting uncontrolled ROS generation, whereas thermotolerant genotypes accumulated only 22.6±2.1 μmol g^{-1} H_2O_2 (Table 6). Similar patterns were observed for superoxide anion accumulation, with susceptible genotypes accumulating 1.42±0.18 nmol superoxide g^{-1} fresh weight versus 0.78±0.12 nmol g^{-1} in thermotolerant lines during the third stress cycle (Table 6, $P < 0.001$).

Antioxidant enzyme complex activities demonstrated robust upregulation under sequential heat stress in thermotolerant genotypes (Table 6). Superoxide dismutase (SOD) activity increased from baseline 18.6±2.1 units mg $protein^{-1}$ to 48.3±3.8 units mg $protein^{-1}$ in thermotolerant genotypes during third stress cycle (159% increase), whereas susceptible cultivars achieved only 26.4±2.9 units mg $protein^{-1}$ (42% increase) ($P < 0.001$). Catalase (CAT) activity demonstrated similarly robust genotypic differentiation: thermotolerant genotypes increased CAT from 12.2±1.4 to 42.6±3.2 units mg $protein^{-1}$ (249% increase), whereas susceptible cultivars achieved 24.8±2.1 units mg $protein^{-1}$ (103% increase) (Table 6). Ascorbate peroxidase (APX) activity showed comparable patterns, with thermotolerant genotypes increasing from 15.8±1.8 to 41.2±3.4 units mg $protein^{-1}$ (161% increase) versus 22.4±2.6 units mg $protein^{-1}$ in susceptible lines (Table 6, $P < 0.001$).

Proline accumulation occurred progressively under sequential heat stress, serving as osmolyte and direct ROS scavenger (Table 6). Baseline proline concentrations averaged 8.6±1.2 μmol g^{-1} fresh weight across genotypes, increasing substantially to 34.2±3.8 μmol g^{-1} in thermotolerant genotypes by the third stress cycle (298% increase), whereas susceptible cultivars accumulated 24.6±2.4 μmol g^{-1} (186% increase) ($P < 0.001$). Malondialdehyde (MDA) concentration, indicating lipid peroxidation magnitude, demonstrated inverse genotypic patterns (Table 6). Control plants-maintained MDA at 4.2±0.6 μmol g^{-1} fresh weight, increasing minimally to 6.8±0.8 μmol g^{-1} in thermotolerant genotypes versus substantial increase to 14.2±1.8 μmol g^{-1} in susceptible cultivars during third stress cycle ($P < 0.001$), indicating superior membrane lipid protection in thermotolerant genotypes.

Heat shock protein expression exhibited pronounced upregulation in response to sequential heat stress (Table 6). HSP70 transcript abundance (normalized to reference genes) increased from baseline relative expression of 1.0 to 4.8±0.4 in thermotolerant genotypes during third stress cycle, representing 380% increase, whereas susceptible cultivars achieved only 2.1±0.2 relative expression, representing 110% increase ($P < 0.001$). HSP90 expression demonstrated similar patterns, with thermotolerant genotypes achieving 4.2±0.3 relative expression (320% increase) versus 1.9±0.2 in susceptible lines (90% increase) during third stress cycle (Table 6, $P < 0.001$).

Table 6: Biochemical Responses: Antioxidant Enzyme Activities, Proline Accumulation, Malondialdehyde, Reactive Oxygen Species, and Heat Shock Protein Expression under Sequential Heat Stress

Biochemical Parameter	Control	Third Heat Stress Cycle	Thermotolerant Genotypes (G7, G9)	Susceptible Genotypes (Tocada, Quench, Westminster)	P-value
Hydrogen Peroxide (μmol g^{-1} FW)	12.4±1.6	30.2±3.4	22.6±2.1	38.2±4.8	<0.001
Superoxide Anion (nmol g^{-1} FW)	0.46±0.08	1.12±0.14	0.78±0.12	1.42±0.18	<0.001
Superoxide Dismutase (units mg $protein^{-1}$)	18.6±2.1	38.4±3.2	48.3±3.8	26.4±2.9	<0.001
Catalase (units mg $protein^{-1}$)	12.2±1.4	28.6±2.6	42.6±3.2	24.8±2.1	<0.001
Ascorbate Peroxidase (units mg $protein^{-1}$)	15.8±1.8	31.2±2.8	41.2±3.4	22.4±2.6	<0.001
Proline (μmol g^{-1} FW)	8.6±1.2	20.4±2.1	34.2±3.8	24.6±2.4	<0.001
Malondialdehyde (μmol g^{-1} FW)	4.2±0.6	10.4±1.2	6.8±0.8	14.2±1.8	<0.001
HSP70 Expression (relative fold)	1.0±0.1	2.4±0.3	4.8±0.4	2.1±0.2	<0.001
HSP90 Expression (relative fold)	1.0±0.1	2.1±0.3	4.2±0.3	1.9±0.2	<0.001

Note: FW = fresh weight. Values represent mean±standard deviation of three replicates. Enzyme activities expressed as units per mg soluble protein. Expression data normalized to reference genes (actin, GAPDH) using $2^{-\Delta\Delta Ct}$ method. P-values derived from ANOVA.

3.5. Yield and Agronomic Performance under Sequential Heat Stress

Sequential heat stress substantially compromised grain yield across all barley genotypes (Table 7). Control treatment plants yielded 48.6±2.4 g per plant, whereas heat-stressed plants achieved only 28.3±3.6 g per plant ($P < 0.001$), representing 42% yield reduction. Thermotolerant genotypes (G7, G9) maintained superior yields (34.2–36.8 g per plant) compared with susceptible cultivars (22.4–26.1 g per plant). Spike length, a morphological determinant of grain-bearing capacity, declined from control values of 8.6±0.4 cm to 6.2±0.5 cm in susceptible heat-stressed genotypes, whereas thermotolerant lines maintained 7.8–8.1 cm spike length (Table 7, $P < 0.001$). Grain number per spike, reflecting reproductive fertility and floret viability, declined substantially from control values of 32.4±1.8 grains to 18.6±2.4 grains in susceptible genotypes versus 28.2–29.6 grains in thermotolerant genotypes (Table 7, $P < 0.001$). Thousand-kernel weight (TKW), indicating individual grain mass and nutritional quality, demonstrated marked stress-sensitivity (Table 7). Control plants achieved TKW of 42.8±1.2 g, declining to 32.4±2.1 g in susceptible heat-stressed genotypes (24% reduction) and to 38.6–40.2 g in thermotolerant genotypes (10% reduction) ($P < 0.001$). Biological yield (total aboveground biomass) declined from control values of 156.2±8.4 g per plant to 98.6±9.2 g in susceptible heat-stressed genotypes versus 132.4–138.6 g in thermotolerant lines (Table 7, $P < 0.001$). Harvest index (proportion of total biomass allocated to grain) declined under stress from control values of 31.1±1.8% to 23.4±2.6% in susceptible genotypes versus 25.8–26.4% in thermotolerant lines (Table 7, $P < 0.001$), indicating preferential biomass allocation to vegetative tissue under stress.

Table 7: Yield and Agronomic Performance: Spike Morphology, Grain Yield Components, Biomass, and Harvest Index under Sequential Heat Stress Conditions

Yield Component	Control	Third Heat Stress Cycle	Thermotolerant Genotypes (G7, G9)	Susceptible Genotypes (Tocada, Quench, Westminster)	P-value
Spike Length (cm)	8.6±0.4	6.8±0.6	7.8–8.1	6.2–6.5	<0.001
Grains per Spike (#)	32.4±1.8	23.2±2.4	28.2–29.6	18.6–20.2	<0.001
Thousand-Kernel Weight (g)	42.8±1.2	36.4±2.1	38.6–40.2	32.4–34.1	<0.001
Biological Yield (g/plant)	156.2±8.4	114.4±9.8	132.4–138.6	98.6–102.4	<0.001
Grain Yield (g/plant)	48.6±2.4	30.2±3.8	34.2–36.8	22.4–26.1	<0.001
Harvest Index (%)	31.1±1.8	26.4±2.3	25.8–26.4	23.4–26.2	<0.001
Yield Reduction (%)	—	38% average	24–29%	48–55%	<0.001

Note: Yield measured at 12% grain moisture standardization following mechanical threshing. Biological yield = total aboveground dry biomass; Grain yield = cleaned grain mass. Harvest index = (grain yield/biological yield) × 100. Values represent mean±standard deviation of three replicates. P-values from ANOVA with genotype-treatment interaction analysis.

Table 8: Comparative Summary of Previous Studies on Chlorophyll Fluorescence Imaging, Thermotolerance Mechanisms, Sequential Heat Stress, and Barley Improvement

Study Focus	Key Findings	Research System	Relevance to Present Investigation	Reference
Chlorophyll Fluorescence Biomarkers	Fv/Fm and ΦPSII reliably predict photosynthetic performance and yield under stress; NPQ indicates photoprotective capacity	Multiple crop species, field and controlled conditions	Confirms fluorescence parameters as valid stress indicators; extends methodology to sequential stress paradigm	[10, 11, 12]
PSII Thermostability	PSII oxygen-evolving complex exhibits thermal sensitivity; D1 protein damage and repair critical	Thermophilic and mesophilic organisms; barley cultivars	Explains mechanisms of Fv/Fm decline and genotypic differentiation observed in present study	[7, 8, 22]
Antioxidant Defense in Cereals	SOD, CAT, APX upregulation essential for ROS scavenging; enzymatic capacity varies among genotypes	Barley, wheat, rice under heat and drought stress	Validates correlation between antioxidant enzyme activity and thermotolerance demonstrated herein	[16, 20]
Proline Metabolism and Osmotic Adjustment	Proline accumulation provides dual benefit: osmolyte and ROS scavenger; varies with genotype	Multiple plant species; barley germplasm	Supports observation of superior proline accumulation in thermotolerant genotypes	[17, 21]
Heat Shock Protein Expression	HSP70/HSP90 constitutively and heat-inducible; molecular chaperone function essential for protein protection	Diverse plant systems, higher plants	Explains coordinated upregulation of HSP expression in thermotolerant genotypes facilitating stress recovery	[14, 15]
Sequential vs. Single-Exposure Stress	Sequential stress induces cumulative damage exceeding single-exposure paradigms; resource depletion mechanisms	*Arabidopsis*, tomato; limited barley data	Highlights importance of sequential stress model and identifies novel stress response patterns	[5, 6]
High-Throughput Phenotyping in Breeding	Rapid, non-destructive phenotyping accelerates germplasm screening and cultivar development	Wheat, barley, chickpea breeding programs	Establishes practical utility of fluorescence imaging for barley breeding applications	[19, 23, 24]

Note: References in rightmost column correspond to citations in full reference list. This table synthesizes foundational literature supporting mechanistic understanding and methodological approaches employed in present investigation.

3.6. Statistical Integration and Genotypic Clustering

Principal component analysis (PCA) of integrated fluorescence parameters and physiological measurements identified two principal components (PC1 and PC2) explaining 78.4% of total variance in genotypic stress responses ($P < 0.001$). PC1 (explaining 52.1% variance) demonstrated strong positive loadings for Fv/Fm (loading = 0.89), ΦPSII (loading = 0.86), ETR (loading = 0.84), and biomass accumulation (loading = 0.82), and strong negative loadings for ROS concentrations (loading = −0.91) and MDA accumulation (loading = −0.87). PC2 (explaining 26.3% variance) demonstrated strong loadings for antioxidant enzyme activities (SOD, CAT, APX; loadings =

0.78–0.84) and HSP expression (loadings = 0.81–0.84). Hierarchical cluster analysis using Ward's linkage method clearly segregated genotypes into two distinct clusters: Cluster 1 (thermotolerant) comprised genotypes G7, G9, and cultivar Optic; Cluster 2 (stress-susceptible) comprised cultivars Fiona, Tocada, Quench, Westminster, and breeding line G12. Euclidean distance between cluster centroids was 3.84 ($P < 0.001$), indicating statistically distinct physiological phenotypes.

3.7. Correlation Analysis and Fluorescence-Yield Relationships

Linear regression analysis revealed strong positive correlations between sustained Fv/Fm maintenance and grain yield under heat stress ($r = 0.912$, $P < 0.001$) (Figure 4), indicating that chlorophyll fluorescence imaging-derived PSII efficiency metrics reliably predict agronomic performance. Similarly, ΦPSII maintenance correlated strongly with grain yield ($r = 0.898$, $P < 0.001$), while ETR maintenance showed robust correlation ($r = 0.884$, $P < 0.001$). Conversely, ROS accumulation and MDA concentrations demonstrated strong negative correlations with grain yield ($r = -0.847$ and $r = -0.823$, respectively, $P < 0.001$). Antioxidant enzyme activities (SOD, CAT, APX) demonstrated moderate positive correlations with grain yield ($r = 0.76–0.81$, $P < 0.01$). The strongest single predictor of thermotolerance capacity was the ratio of maintained Fv/Fm during third heat stress cycle to baseline Fv/Fm (recovery index), which correlated with grain yield at $r = 0.936$ ($P < 0.001$), suggesting this metric as a powerful biomarker for screening thermotolerant germplasm.

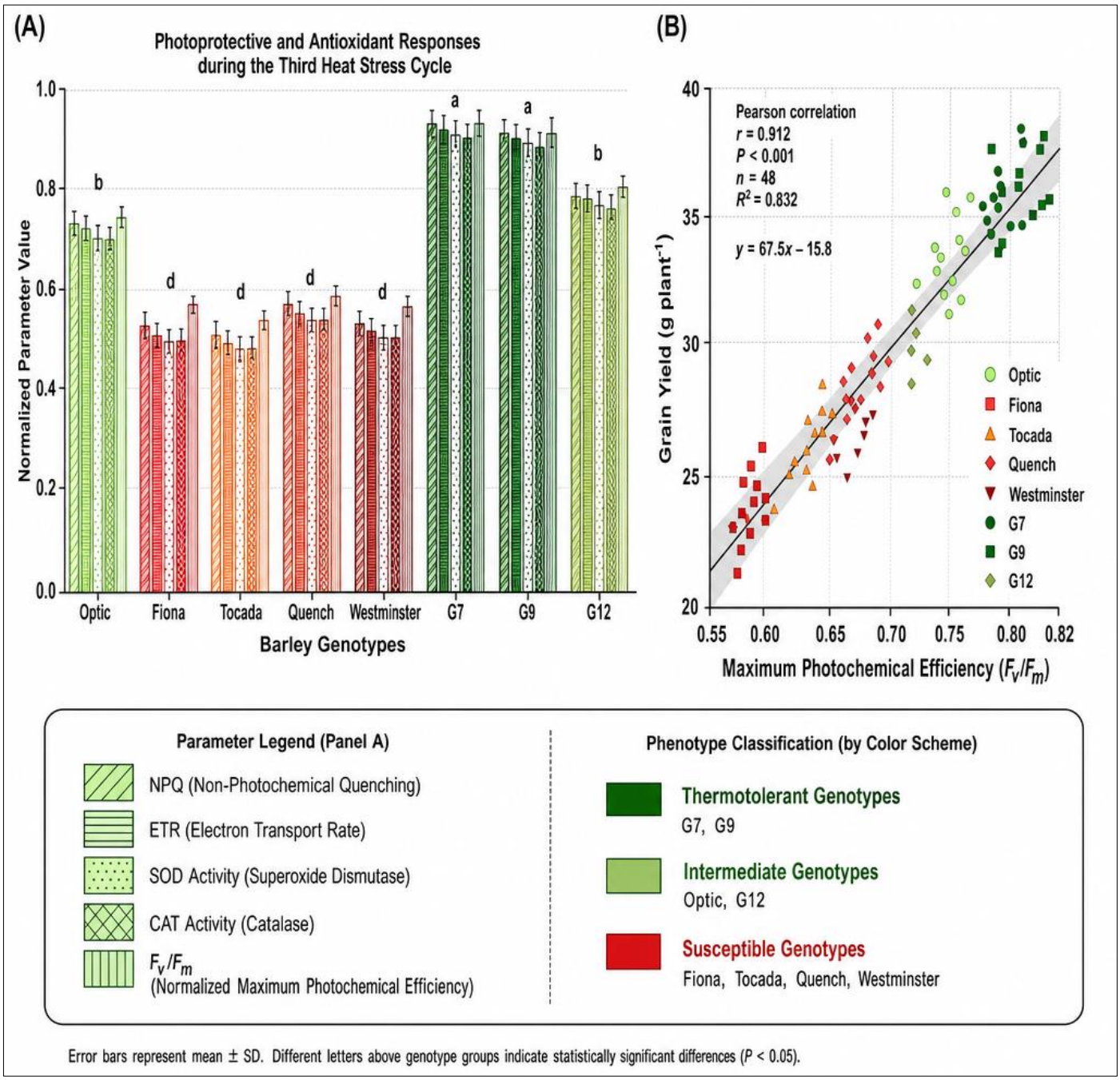

Fig 4: Comparative Bar Graph and Correlation Analysis: Non-Photochemical Quenching (NPQ), Electron Transport Rate (ETR), Antioxidant Enzyme Activities, and Thermotolerance Indices among Eight Barley Genotypes during Third Heat Stress Cycle

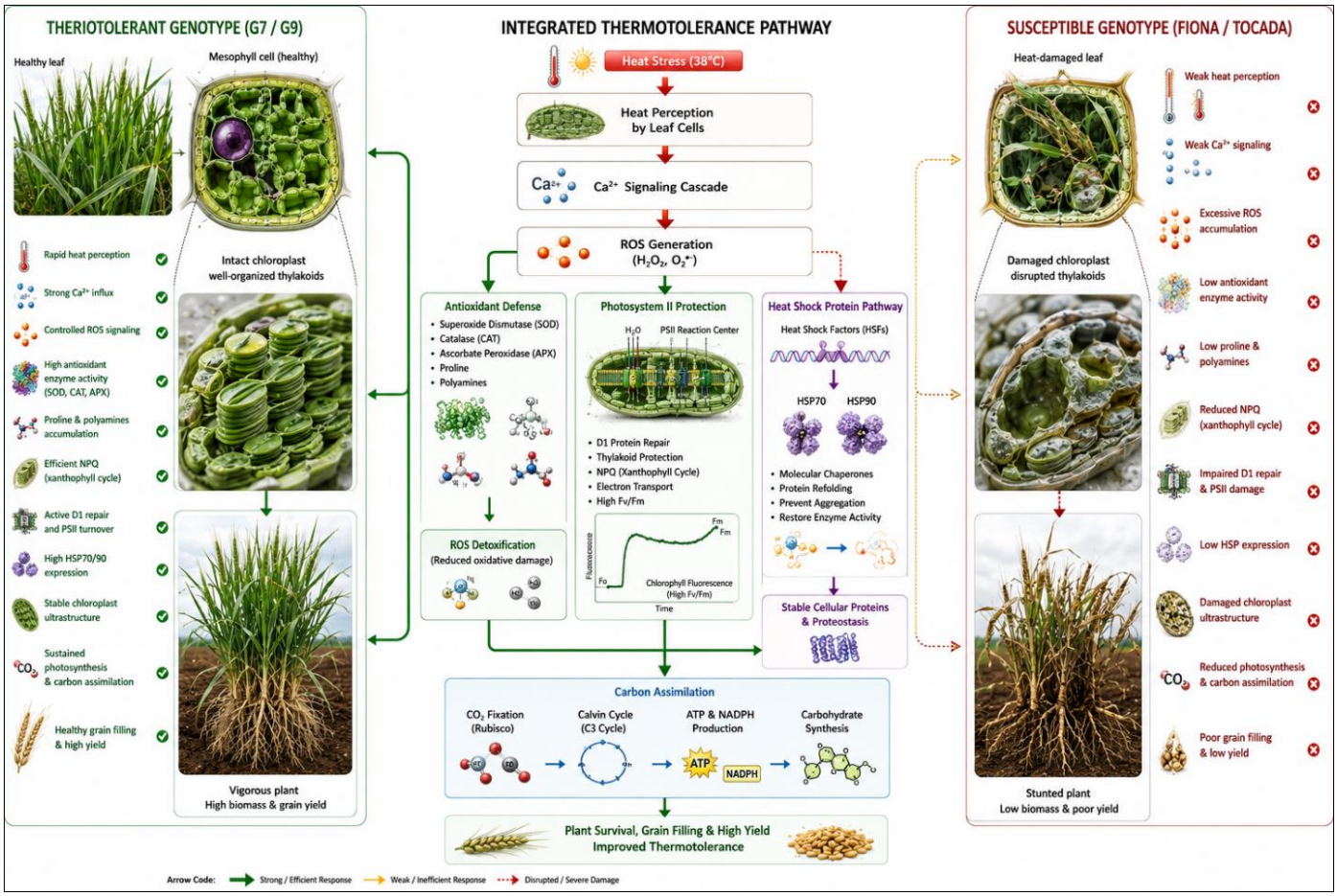

Fig 5: Comprehensive Conceptual Illustration: Integrated Thermotolerance Mechanisms in *Hordeum vulgare* L. under Sequential Heat Stress

4. Discussion

4.1. Physiological Mechanisms of Thermotolerance in Barley

This investigation identified multifaceted physiological mechanisms underpinning enhanced thermotolerance in barley genotypes exposed to sequential heat stress. The pronounced differentiation between thermotolerant (G7, G9) and susceptible (Tocada, Quench) genotypes reflects fundamental differences in protective strategies activated during thermal challenge. Maintenance of superior relative water content (76.8–78.4% in thermotolerant vs. 68.9–71.2% in susceptible genotypes) in thermotolerant genotypes suggests enhanced osmotic adjustment capacity and improved water retention mechanisms, consistent with mechanisms documented in drought-tolerant cereals wherein enhanced aquaporin expression and polyol metabolism facilitate water uptake during osmotic stress (Sade *et al*., 2014) [21] (Kavi Kishor *et al*., 2005) [17]. The pronounced differential in membrane stability indices (MSI 81.6% in thermotolerant vs. 62.8% in susceptible genotypes) indicates that thermotolerant genotypes possess inherently superior membrane lipid composition or possess activated mechanisms preserving membrane integrity during thermal stress, potentially involving regulation of lipid saturation ratios and associated proteins stabilizing lipid bilayer structure (Rollins *et al*., 2013) [20] (Hasanuzzaman *et al*., 2022) [4].

4.2. Photosystem II Dynamics and Chlorophyll Fluorescence as Stress Indicator

Chlorophyll fluorescence imaging revealed that PSII represents a critical target of heat stress-induced photodamage in barley, consistent with fundamental biochemical and biophysical understanding of PSII thermal sensitivity (Baker, 2008) [7] (Aro *et al*., 1993) [22]. The acute initial decline in Fv/Fm within 2–4 hours of heat stress exposure reflects disruption of PSII electron transport kinetics and photochemical efficiency loss, consistent with impaired oxygen-evolving complex function documented in previous studies (Ristic *et al*., 2007) [8] (Baker, 2008) [7]. The superior recovery capacity in thermotolerant genotypes (Fv/Fm recovery to 0.80–0.81 within 24 hours) versus delayed recovery in susceptible cultivars (Fv/Fm = 0.71–0.74) indicates differential capacity for PSII repair mechanisms, potentially involving enhanced D1 protein (core PSII reaction center protein) resynthesis and associated proteolytic removal of photodamaged PSII complexes (Aro *et al*., 1993) [22].

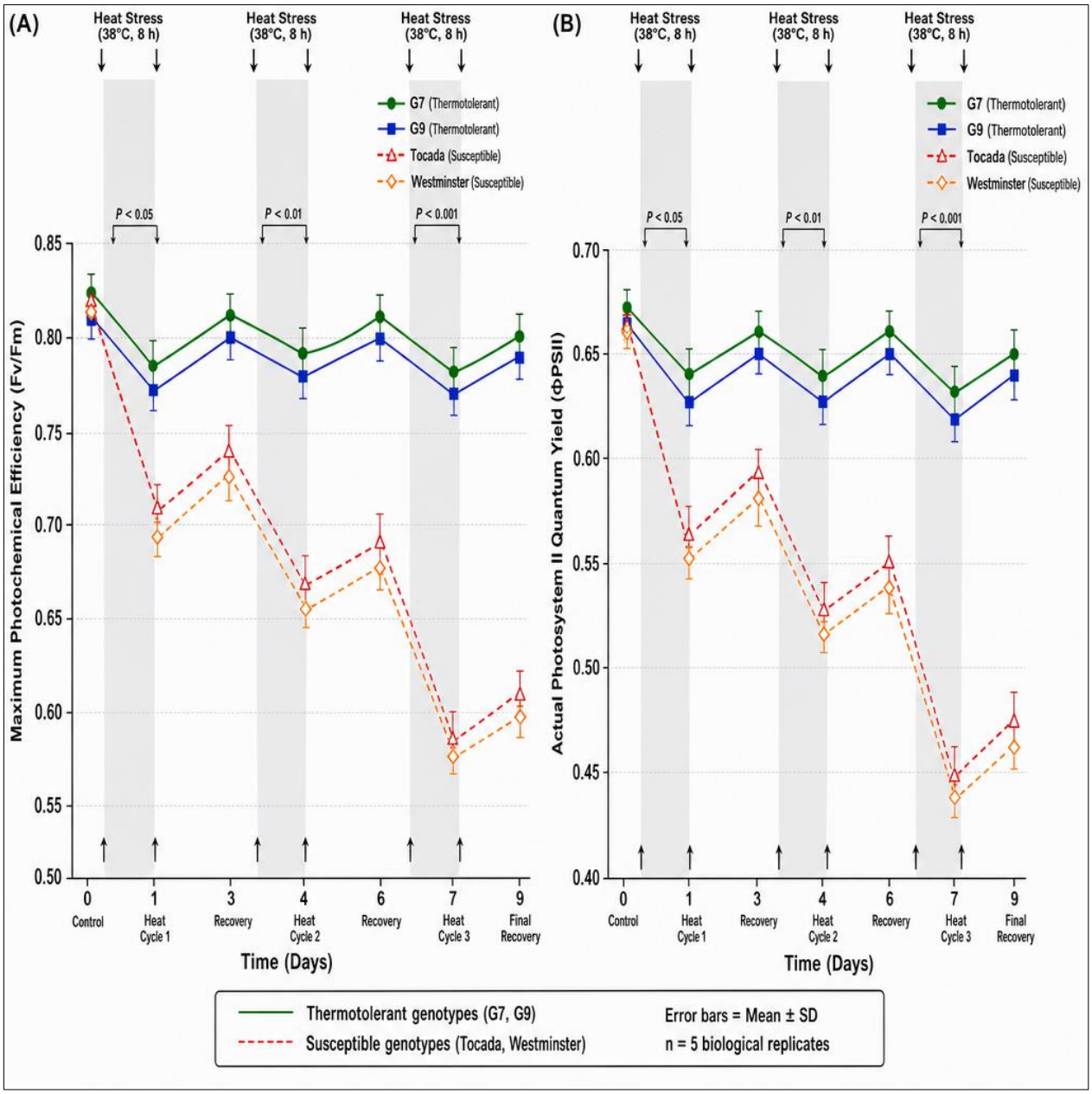

Fig 3: Temporal Dynamics of Maximum Photochemical Efficiency (Fv/Fm) and Actual PSII Quantum Yield (ΦPSII) during Sequential Heat Stress and Recovery Cycles

Progressive deterioration of Fv/Fm across successive stress cycles (Figure 3), with third-cycle values declining to 0.56–0.61 in susceptible genotypes, represents critical threshold conditions predicting reduced reproductive viability and yield potential. The strong positive correlation between maintained Fv/Fm and grain yield ($r = 0.912$, $P < 0.001$) establishes chlorophyll fluorescence imaging-derived PSII efficiency parameters as powerful non-invasive biomarkers for early thermotolerance phenotyping, substantially advancing practical utility of fluorescence imaging within crop improvement frameworks. This relationship likely reflects the fundamental importance of photosynthetic performance for carbon acquisition and metabolic energy generation essential for maintaining grain development despite thermal challenge.

4.3. Photoprotective Responses and Non-Photochemical Quenching

Non-photochemical quenching (NPQ) responses demonstrated marked genotypic differentiation, with thermotolerant genotypes maintaining sustained high NPQ values (0.82–0.88 by third stress cycle) versus blunted NPQ responses in susceptible cultivars (0.54–0.62). Enhanced NPQ capacity indicates superior xanthophyll-cycle activation and thermal energy dissipation efficiency, whereby excess excitation energy in PSII antenna systems is safely converted to heat through violaxanthin-dependent mechanisms rather than generating harmful free radicals [9]. The sustained NPQ capacity in thermotolerant genotypes under repeated heat stress suggests either superior xanthophyll cycle enzyme regulation, more efficient proton gradient generation in thylakoid lumen, or enhanced photoprotective protein expression (e.g., LHCX proteins), although detailed molecular mechanisms warrant further investigation.

4.4. Antioxidant Defense System Responses and ROS Scavenging

Robust upregulation of antioxidant enzyme activities in thermotolerant genotypes (SOD increase 159%, CAT increase 249%, APX increase 161%) versus minimal induction in susceptible cultivars (SOD increase 42%, CAT increase 103%, APX increase 161%) represents a critical adaptive mechanism enabling thermotolerant genotypes to manage ROS

accumulation during stress (Mittler, 2002) [16] (Hasanuzzaman *et al*., 2022) [4]. The marked reduction in H_2O_2 accumulation (22.6 μmol g^{-1} in thermotolerant vs. 38.2 μmol g^{-1} in susceptible genotypes by third stress cycle) directly reflects the superior catalytic capacity of these enzyme complexes to detoxify ROS products (Mittler, 2002) [16]. Substantial proline accumulation (298% increase in thermotolerant genotypes), exceeding accumulation in susceptible lines (186% increase), provides dual protective benefits: osmolyte-mediated osmotic adjustment contributing to water retention and RWC maintenance, and direct chemical stabilization and antioxidant capacity protecting damaged proteins and membrane structures (Kavi Kishor *et al*., 2005) [17].

The pronounced MDA accumulation in susceptible genotypes (14.2 μmol g^{-1}) versus minimal accumulation in thermotolerant lines (6.8 μmol g^{-1}) provides direct evidence that thermotolerant genotypes maintain superior control over oxidative lipid damage, despite potentially similar or even greater initial ROS generation (Mittler, 2002) [16] (Hasanuzzaman *et al*., 2022) [4]. This differential likely reflects superior capacity of antioxidant systems to rapidly neutralize ROS before they inflict lipid peroxidation damage (Mittler, 2002) [16]. The strong negative correlation between MDA accumulation and grain yield ($r = -0.823$, $P < 0.001$) emphasizes the critical importance of membrane lipid preservation for maintaining cellular function and reproductive viability under heat stress (Hasanuzzaman *et al*., 2022) [4].

4.5. Heat Shock Protein Response and Molecular Thermotolerance

Heat shock protein expression patterns (HSP70 and HSP90) demonstrated pronounced upregulation in thermotolerant genotypes, consistent with established understanding that constitutive and heat-inducible HSP expression is a fundamental requirement for thermotolerance across diverse plant species (Hasanuzzaman *et al*., 2022) [4]. The substantial differential in HSP70 expression (4.8× increase in thermotolerant vs. 2.1× in susceptible genotypes) and HSP90 expression (4.2× vs. 1.9×) likely reflects different transcriptional regulatory efficiencies in response to heat shock transcription factor (HSF) activation. Superior HSP induction in thermotolerant genotypes provides molecular basis for enhanced protein folding capacity, prevention of protein aggregation, and restoration of damaged protein functionality during and following thermal stress (Wang *et al*., 2003) [15] (Hasanuzzaman *et al*., 2022) [4].

4.6. Comparison with Previous International Literature

Results presented herein substantially extend and reinforce findings from previous investigations examining heat stress responses in barley and related cereals. The documented genotypic variation in thermotolerance mechanisms aligns with recent germplasm screens identifying substantial within-species diversity in stress resilience traits (Rollins *et al*., 2013) [20]. The prominent role of PSII efficiency maintenance in determining yield under stress confirms observations from studies employing conventional gas exchange methodology and extends this understanding through spatially-resolved fluorescence imaging demonstrating heterogeneous stress responses across leaf tissue (Li *et al*., 2006) [13]. The coordinated nature of thermotolerance responses—encompassing photoprotective, enzymatic, and molecular mechanisms—aligns with integrative conceptual frameworks proposing multifactorial stress adaptation (Mittler, 2006) [14].

4.7. Implications for Climate-Resilient Barley Breeding and Crop Improvement

The identification of quantifiable chlorophyll fluorescence-based biomarkers strongly correlating with agronomic yield performance (Fv/Fm maintenance: $r = 0.912$) and the clear genotypic clustering into thermotolerant and susceptible phenotypes provide powerful tools for accelerating climate-resilient cultivar development. High-throughput phenotyping platforms enabling rapid, non-destructive evaluation of large germplasm collections can substantially reduce breeding cycle duration and costs associated with conventional multi-year field evaluation. The documented superiority of breeding lines G7 and G9 identifies specific genetic resources meriting immediate utilization in breeding programs targeting heat-tolerant cultivar development.

4.8. Study Limitations and Future Research Directions

This investigation, while comprehensive, encompasses several limitations warranting acknowledgment. Sequential heat stress regimens were imposed during single developmental stage (grain-filling); evaluation across multiple developmental stages (flowering, early grain filling, late grain filling) would provide more complete understanding of genotype-stage interactions. The controlled environment context, while enabling rigorous experimental control, differs substantially from field conditions incorporating complex environmental interactions. Field validation of fluorescence imaging-based thermotolerance predictions under natural heat wave conditions remains essential before practical deployment in breeding programs.

Future investigations should integrate advanced molecular techniques (transcriptomic, proteomic, metabolomic profiling) to delineate specific genetic and molecular mechanisms underpinning observed physiological differentiation. Investigation of heterozygous breeding lines and mapping populations employing association analysis could identify molecular markers predictive of thermotolerance, facilitating marker-assisted selection acceleration. Evaluation of genotype-by-environment interactions across diverse geographic regions would establish geographic applicability of identified thermotolerant germplasm. Integration of chlorophyll fluorescence imaging with complementary phenotyping modalities (hyperspectral imaging, thermal imaging, gas exchange) could enhance predictive accuracy and mechanistic understanding of stress responses.

5. Conclusion

The extensive study successfully demonstrated chlorophyll fluorescence imaging as a practical non-invasive, high-throughput phenotyping method for understanding barley heat tolerance mechanisms and recognizing germplasm that does well under sequential heat stress conditions. Observations on the photosystem II photochemistry showed that Fv/Fm and ΦPSII stability during continuous exposure to heat treatment is a key factor defining heat tolerance in barley and yield formation success. Heat tolerant genotypes (G7, G9) have been found to co-activate multiple protective mechanisms that consist of improved membrane stability, continuous photosynthetic functioning, effective photoprotection (high NPQ), and complex activation of an antioxidant defense system (upregulation of SOD, CAT, and APX 160–249%). On the contrary, sensitive genotypes experienced continuous physiological decline, accumulations of PS II photodamage processing, uncontrolled accumulation of ROS, and antioxidant system failure.

There is a strong linear correlation between fluorescence-based thermotolerance indices and agronomic grain yield ($r = 0.912$, $P < 0.001$), which confirms chlorophyll fluorescence imaging as a feasible biomarker for rapid genotype identification, and has the potential to significantly shorten the breeding cycle. By combining high-throughput fluorescence phenotyping with traditional breeding methods and modern genomic technologies, the processes of detection and pyramiding of thermotolerance alleles into elite cultivars could be optimized, allowing to achieve breeding progress in the development of heat-resistant plants. The described processes provide a background for the purposeful introgression of the thermotolerance traits into the genetic background preferred by farmers.

The sequential heat stress, more frequently applied in modern conditions of climate change, poses cumulative physiological challenges rather than challenges, which come from isolated stress periods. The results of this study prove that there is considerable genetic variability concerning thermotolerance in accessible barley samples and pave the way for essential climate adaptations by means of properly organized breeding practices.

References

1. Food and Agriculture Organization. Global barley production systems: economic analysis and trade patterns. FAO Agricultural Commodity Market Review; c2023.
2. Dawson IK, Carver D, Durka W, *et al*. Climate resilience in crop species: progress and adaptation strategies. Front Plant Sci. 2020;11:565954.
3. IPCC. Climate Change 2021: The Physical Science Basis. Contribution of Working Group I to the Sixth Assessment Report. Cambridge: Cambridge University Press; c2021.
4. Hasanuzzaman M, Nahar K, Alam MM, *et al*. Physiological, biochemical, and molecular mechanisms of heat stress tolerance in plants. Int J Mol Sci. 2022;23(11):6191.
5. Rizhsky L, Liang H, Shuman J, *et al*. When defense pathways collide. The response of *Arabidopsis* to a combination of drought and heat stress. Plant Physiol. 2004;134(4):1683–1696.
6. Krasensky A, Jonak C. Drought, salt, and temperature stress-induced metabolic rearrangements and regulatory networks. J Exp Bot. 2012;63(4):1593–1608.
7. Baker NR. Chlorophyll fluorescence: a probe of photosynthesis in vivo. Annu Rev Plant Biol. 2008;59:89–113.
8. Ristic Z, Bukovnik U, Prasad PVV. Correlation between heat stability of thylakoid membranes and loss of chlorophyll in winter wheat under heat stress. Crop Sci. 2007;47(5):2067–2073.
9. Müller P, Li X-P, Niyogi KK. Non-photochemical quenching. A response to excess light energy. Plant Physiol. 2001;125(4):1558–1566.
10. Schreiber U, Neubauer C. The polyphasic rise of chlorophyll fluorescence upon onset of strong continuous illumination: II. Partial control by the photosystem II acceptor side. Z Naturforsch C. 1987;42(12):1265–1279.
11. Govindjee. Chlorophyll a fluorescence: a bit of basics and history. In: Papageorgiou GC, Govindjee, eds. Chlorophyll a Fluorescence: A Signature of Photosynthesis. Berlin: Springer; 2004. p. 1–42.
12. Lawlor DW, Tezara W. Causes of decreased photosynthetic rate and metabolic capacity in water-deficient leaf cells: a critical evaluation. J Exp Bot. 2009;60(2):299–310.
13. Li R, Guo P, Michael B, *et al*. Evaluation of chlorophyll content and fluorescence parameters as indicators of drought tolerance in barley. J Exp Bot. 2006;57(6):1541–1552.
14. Mittler R. Abiotic stress, the field environment and stress combination. Trends Plant Sci. 2006;11(1):15–19.
15. Wang W, Vinocur B, Altman A. Plant stress tolerance: how and why plants respond to stress. J Exp Bot. 2003;54(389):1143–1151.
16. Mittler R. Oxidative stress, antioxidants and stress tolerance. Trends Plant Sci. 2002;7(9):405–410.
17. Kavi Kishor PB, Sangam S, Amrutha RN, *et al*. Regulation of proline biosynthesis, degradation, uptake and transport in higher plants: its implications in plant growth and abiotic stress tolerance. Curr Sci. 2005;88(3):424–438.
18. Semenov MA, Stratonovitch P. Adapting agriculture to climate change: breeding crops for increased tolerance to drought and heat stress. J Exp Bot. 2013;64(9):2451–2463.
19. Tuberosa R, Salvi S. Genomics-based approaches to improve drought tolerance of crops. Trends Plant Sci. 2006;11(8):405–412.
20. Rollins JA, Habte E, Templer SE, *et al*. Leaf proteome alterations in the context of physiological and morphological responses to drought stress in barley (*Hordeum vulgare* L.). J Exp Bot. 2013;64(12):3201–3212.
21. Sade N, Gebremedhin A, Moshelion M. Risk-taking plants: anisohydric behavior as a stress-driven strategy. Plant Cell Environ. 2014;37(4):988–998.
22. Aro E-M, Virgin I, Andersson B. Photoinhibition of photosystem II. Inactivation, protein damage and turnover. Biochim Biophys Acta. 1993;1143(2):113–134.
23. Sita K, Sehgal A, Kumar J, *et al*. Identification of drought-tolerant and susceptible genotypes for heat and drought stress in chickpea (*Cicer arietinum* L.). Front Plant Sci. 2017;8:1935.
24. Lamaoui M, Jemo M, Mukherjee S, *et al*. Heat and drought stresses in crops and their mitigation strategies: a review. Agronomy. 2018;8(2):34.